



Physical and Chemical Properties of Poly(ethylene)oxide Ternary Solid Polymer Electrolytes Based on Ni/Al Layered Double Hydroxide

SITI NURUL 'AFINI MOHD JOHARI¹, SITI KHATIJAH DERAMAN^{2,*}, HUSSEIN HANIBAH² and NAZRIZAWATI AHMAD TAJUDDIN¹

¹School of Chemistry and Environment, Faculty of Applied Sciences, Universiti Teknologi MARA, 40450 Shah Alam, Selangor, Malaysia

²Centre of Foundation Studies, Universiti Teknologi MARA, Cawangan Selangor, Kampus Dengkil 43800 Dengkil, Selangor, Malaysia

*Corresponding author: E-mail: drsitikhatijah@uitm.edu.my

Received: 24 May 2024;

Accepted: 3 July 2024;

Published online: 30 August 2024;

AJC-21729

In this work, a solid polymer electrolyte (SPE) was synthesized by solution casting technique using poly(ethylene oxide) (PEO) as polymer host doped with lithium trifluoromethanesulfonate (LiCF_3SO_3) and Ni/Al layered double hydroxide (Ni/Al LDH) as filler. Subsequently, Ni/Al LDH were introduced into the polymer electrolyte and characterized by electrochemical impedance spectroscopy (EIS) to determine the composition of additive, which gives the highest conductivity for each system. At ambient temperature, the highest conductivity is obtained for the composition PEO-5 wt.% Ni/Al LDH-8 wt.% LiCF_3SO_3 with a value $8 \times 10^{-6} \text{ S cm}^{-1}$. X-ray diffraction (XRD) studies indicate that the conductivity increase is due to an increase in amorphous content which enhances the segmental flexibility of polymeric chains and the disordered structure of the electrolyte. For composites, the characteristic peaks of Ni/Al LDH disappeared irrespective of filler content. The presence of complexation and interaction among the components was demonstrated by FTIR spectra, while images captured by FESEM revealed the morphological changes in the solid polymer electrolyte.

Keywords: Solid polymer electrolyte, Solution casting technique, Ionic conductivity, Layered double hydroxide, Hydrotalcites.

INTRODUCTION

Electrolytes are compounds that possess inherent positive or negative electrical charges when they are dissolved in water [1]. Polymer electrolytes (PEs) are salts which are incorporated into a polymer matrix, causing the salt to separate into individual ions and get attached to the polymer backbone, particularly at the chemically active point of the polymer backbone. Salt facilitates the movement of ions, whereas the polymer serves as the medium for ion mobility [2]. Many workers have extensively examined the different systems of PEs to get an ideal electrolyte system. There are three distinct categories of PEs: liquid polymer electrolyte (LPE), gel polymer electrolyte (GPE) and solid polymer electrolyte (SPE).

Solid polymer electrolytes (SPEs) are typically membranes formed by dissolving salt in a polymer matrix at room temperature. The introduction of SPE was first studied by Fenton *et al.* in 1973 and its significance was acknowledged in early 1980s by Armand [3]. Recently, there has been extensive use of SPEs in the advancement of lithium-ion batteries with

high energy density. This poses a difficulty for bigger applications such as electric cars and smart grids [4,5]. Solid polymer electrolyte (SPE) is often used in rechargeable lithium-ion batteries, which are commonly used in consumer portable electronic and communications devices [6].

Secondary lithium-ion batteries are now focusing significant attention on SPEs for their potential extensive use. Research on solid polymer electrolytes (SPE) has been primarily concentrated since 1973, when Wright [7] first documented the phenomenon of ionic conduction in the complex formed by polymers and salts. The benefits of solid polymer electrolyte (SPE) have sparked significant attention among researchers. These advantages include the absence of electrolyte leakage, high energy density, flexible geometry, excellent cyclability, strong mechanical strength and enhanced safety [8]. Various techniques have been devised to enhance the mechanical, morphological and ionic conductivity of polymer electrolytes. These include inorganic fillers [9], plasticizers [10] and modifying the polymer structure [11]. Recently, there has been growing interest in incorporating inorganic fillers into solid polymer electrolytes

(SPEs) because these fillers provide improved mechanical stability and higher ionic conductivity, which in turn leads to greater stability at the electrolyte-electrolyte interface. The objective is to enhance the mechanical strength of solid polymer electrolytes (SPEs) by achieving a uniform distribution of inorganic fillers inside them. Previous research has firmly shown that the inclusion of inorganic fillers enhances the conductivity of polymer host, which has a range of 10^{-8} – 10^{-5} S cm^{-1} . Additionally, these fillers also increase the interfacial characteristics of polymer when it comes into contact with salts [12,13].

The polymer host for this investigation will be high molecular weight polyethylene oxide (PEO). PEO is considered the optimal host polymer matrix, since it has the ability to dissolve in a diverse range of lithium salts and additives [14]. Moreover, PEO has enhanced ionic conductivity compared to other polymers due to the formation of stable electrolytic complexes [15]. The PEO material has excellent optical transparency, chemical resistance and surface resistance. The morphological structure of PEO complexed with salts has a crucial role in determining the transit of ions inside the material [16]. Due to the presence of helical structure consisting of C-O and C-C bonds in PEO, which is highly structured, having both crystalline and amorphous phases. Additionally, PEO exhibits strong complexation and mechanical stability. Nevertheless, the presence of crystalline PEO phase restricts the movement of ions along the polymer chains in a specific region. Therefore, without further optimization with electrochemical applications, PEO-based electrolytes have a room temperature ionic conductivity of 10^{-7} S cm^{-1} [17].

Lithium trifluoromethanesulfonate (LiCF_3SO_3) will be used as doping salt. This salt exhibits exceptional solubility, remarkable ionic conductivity and outstanding electrochemical stability. The dissociation of this lithium salt, which contains significant anions, is facilitated inside the PEO matrix, leading to the release of lithium cations and thus enhancing the ionic conductivity [18]. Recently, LDHs have garnered significant interest because to their diverse and significant uses in catalysis, photochemistry, electrochemistry, magnetization, medicinal research and environmental applications. LDHs possess a substantial surface area, a high anion exchange capacity that is equivalent to that of anion exchange resins and exhibit commendable thermal stability [19]. The inorganic fillers used for this purpose will be nickel/aluminum layered double hydroxide (Ni/Al LDH). Therefore, the study on the combined effect of LiCF_3SO_3 and Ni/Al LDH on PEO would be the great interest. This work has been driven by a desire to investigate the properties of PEO-based nanocomposite PEs in achieving high ionic conductivity promoted by LiCF_3SO_3 and Ni/Al LDH at various ratio.

EXPERIMENTAL

Tetrahydrofuran (THF) and acetonitrile (ACN) with HPLC grade were supplied by R&M Chemicals, Malaysia. Polyethylene oxide (PEO) ($M_n \sim 4,000$ Kg mol^{-1}) (>99% pure), was supplied by Aldrich Chemicals, USA. Lithium trifluoromethanesulfonate (LiCF_3SO_3) (>97% pure) was supplied by Alfa Aesar, USA. All the mentioned product been used without any further purification in this research.

Preparation of polymer electrolytes: The polymer electrolytes (PEs) were prepared *via* solvent casting technique. Polyethylene oxide (PEO, 1.0 g) was dissolved in 50 mL of ACN. Different ratio of fresh, calcined Ni/Al LDH and LiCF_3SO_3 (wt.%) were added into the polymer solutions system. Then, the mixtures were continuously stirred at 50 °C for 24 h to obtain a homogeneous and transparent solutions. The solutions were cast into Teflon petri dishes and left to dry for 2 days to form a free standing film. All the samples were prepared at ambient temperature and then stored in desiccator. The SPE system that consists of PEO–FNi/Al LDH, PEO–CNi/Al LDH and PEO– LiCF_3SO_3 were prepared and analyzed accordingly

Characterization: X-ray diffraction (XRD) performed by PANalytical X'pert PRO model was operated at 40 kV and 40 mA using $\text{CuK}\alpha$. Measurements were made with diffraction angle 2θ from 8 to 90 °C at speed $1.2^\circ \text{min}^{-1}$. Fourier transform infrared (FTIR) analysis was used to determine the structure confirmation of polymer electrolyte structure and its functional groups in PEO–Ni/Al LDH, PEO– LiCF_3SO_3 and PEO– LiCF_3SO_3 –Ni/Al LDH. FTIR were performed using Perkin-Elmer model spectrum one spectrometer (USA) in the range 4000–600 cm^{-1} with ATR mode. The surface morphologies of the synthesized materials of the polymer electrolytes were studied using field emission scanning electron (FESEM) on a Jeol JSM-7600F instrument with a Schottky emitter at an accelerating voltage of 2.0 kV with a beam current of 1.0 mA. The samples were ultrasonically dispersed in ethanol and deposited Au-coated silicon chips prior to analysis. Electrochemical impedance spectroscopy (EIS) was used to determine the electrical characterization of the polymer electrolyte films. The polymer electrolyte films of known thickness were sandwiched between to aluminum blocking electrodes with contact area of 7.9 cm^2 . The ionic conductivity of the polymer electrolytes has been measured at ambient temperature using computer-interfaced HIOKI HiTester (Japan) impedance analyzer in the frequency range of 42 Hz to 5 MHz by applying the potential of 1.1 V.

RESULTS AND DISCUSSION

PEO electrolyte system

Effect of solvent on PEO electrolyte system: In this study, high molecular weight PEO was dissolved in different polarity (μ) solvent system at the ambient temperature. PEO with different concentrations was dissolved separately using these three solvents *viz.* water, ACN and THF. The optimum conductivity for the system was identified before further addition with Ni/Al LDH and LiCF_3SO_3 at ambient temperature. Subsequently, the solution was also prepared using the solvent casting process. It is crucial to ascertain the most effective electrolyte system for PEO. Upon visual inspection, it was found that the PEO solution with a concentration of 2 (wt./wt.%) in all three solvents forms a homogenous solution without any phase separation at room temperature. It should be mentioned that PEO forms a heterogeneous (reprecipitation) solution when its concentration exceeds 2 wt./wt.% in all solvent systems. In addition, PEO with a concentration lower than 2 wt./wt.% was not selected due to inadequate physical and mechanical film qualities during the

casting process. Fig. 1 displays the independent film of PEO with several solvent systems at a concentration of 2% by weight.

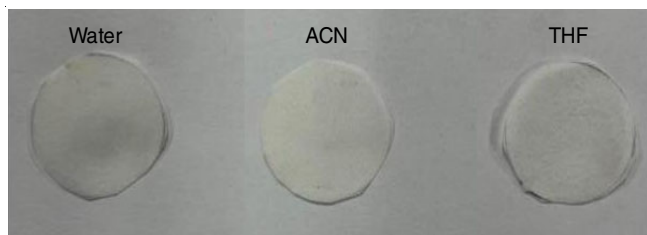


Fig. 1. Free standing PEO film in different solvent systems

Ionic conductivity of PEO system in different solvent were observed for all the free standing film. It is observed that the ionic conductivity (σ) for all three system shows a similar magnitude conductivity that approaching σ of pure PEO (10^{-9} S cm^{-1}) at ambient temperature [20,21]. The differences of σ for pure PEO with PEO in different solvent system shows a minimum difference. This result is expected mainly due to the lack of free moving ion charge (charge carrier) in this system. From the conductivity measurement for all the three system as 2.63×10^{-9} S cm^{-1} (H_2O), 1.76×10^{-9} S cm^{-1} (ACN) and 1.47×10^{-9} S cm^{-1} (THF). It shows that H_2O give the highest σ compared to ACN and THF. This is mainly due to the properties of this universal solvent behaviour. As mentioned earlier, H_2O has the higher dielectric constant (ϵ) as compared to ACN and THF [22]. Nevertheless, the inclusion of PEO in the H_2O system has not been selected for further examination in order to establish a PEO electrolyte system. The primary rationale for not selecting water is attributed to the challenge of obtaining a fully self-supporting PEO film. This is due to the films' sluggish drying rate, which results in the formation of a fully dried film taking almost a month. This is mostly due to the high hydrogen bonding potential of PEO in solution. Consequently, a greater amount of energy is required to counteract this attractive force and create a fully dehydrated film [23]. Moreover, this technique is unsuitable for studying electrolytes, especially in battery applications, since it primarily induces electrode corrosion [24]. Thus, it may be inferred that the H_2O electrolyte system is unsuitable for further analysis in this research.

Therefore, the further analysis was narrow down only focus on ACN and THF to prepare the electrolyte system at ambient temperature. It shows that ACN has higher ionic conductivity (σ) compared to THF. This is mainly due to higher ϵ and μ of ACN ($\epsilon = 36.64$, $\mu = 0.46$) and THF ($\epsilon = 7.52$, $\mu = 0.207$) [25]. As observed earlier, the σ of ACN-PEO system shows a higher value compared to THF-PEO system. Therefore, ACN has been chosen as solvent to dissolve the PEO to prepare the SPE system for the remaining study.

Physico-chemical studies of PEO system X-ray diffractions (XRD) of the system

PEO-Ni/Al LDH: The XRD patterns of PEO are shown in Fig. 2. The XRD of PEO contains two sharp diffraction peaks at 19.19° and 23.63° which are assigned to set of planes (120) and (112) that are confirmed the semicrystalline nature of PEO

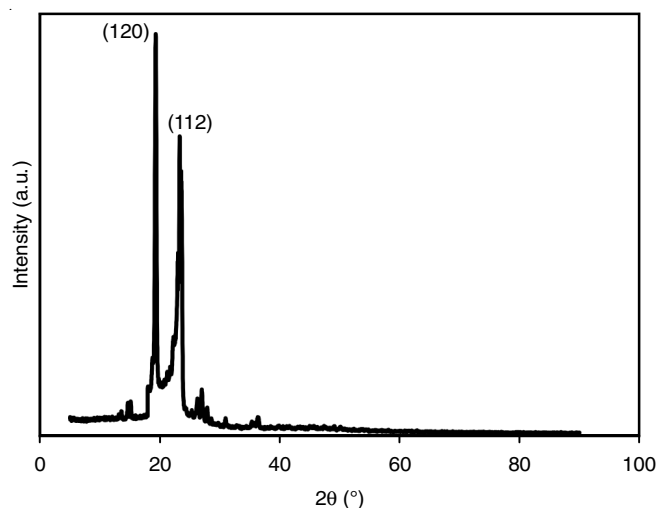


Fig. 2. X-ray diffraction patterns of the PEO

[26]. Consequently, the impact of Ni/Al LDH on the crystallinity region of PEO was further investigated. After undergoing heat treatment, only 5 wt.% of FNi/Al LDH and CNi/Al LDH were used. These LDHs were then doped into the PEO system utilizing the solvent casting process.

Fig. 3 displays the XRD patterns of the PEO-FNi/Al and CNi/Al LDH. It is evident that the inclusion of FNi/Al LDH and CNi/Al LDH in PEO results in the formation of a self-supporting film. There are no noticeable changes in the strength of the semicrystalline peaks of PEO before and after doping with LDH. This suggests the absence of any further intermolecular interaction between polyethylene oxide (PEO) and layered double hydroxide (LDH), which might be attributed to the absence of lamella structure breakdown in the crystalline PEO area [27]. LDH does not contribute to or improve the overall amorphous region of the system, as it does not increased the conductivity. Therefore, the impact of adding LiCF_3SO_3 on the crystallinity behaviour of the system has been investigated.

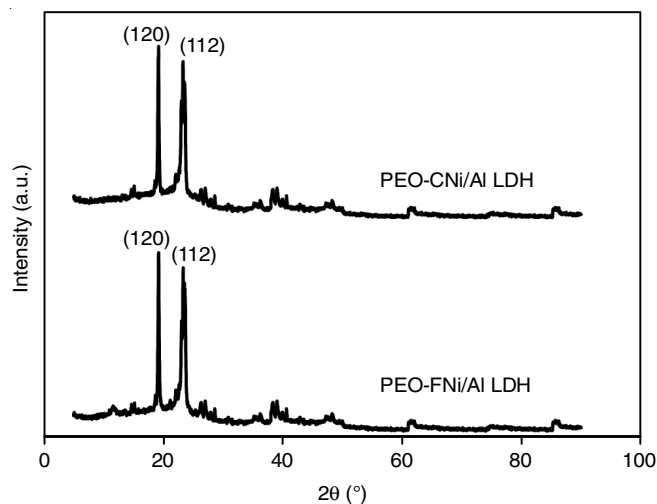


Fig. 3. X-ray diffraction patterns of PEO-Ni/Al LDH

PEO-LiCF₃SO₃: Fig. 4 exhibits the XRD patterns of the PEO-LiCF₃SO₃ and it was observed that few crystalline peaks of the PEO substantially shifted in intensity upon increasing

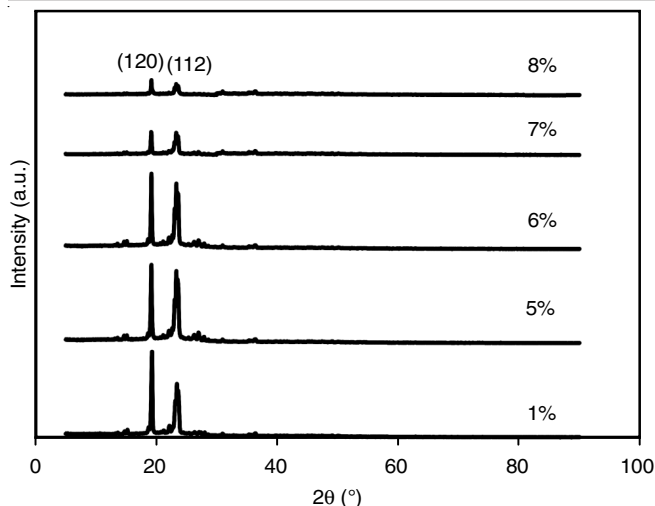


Fig. 4. X-ray diffraction patterns of PEO-LiCF₃SO₃

the concentration of LiCF₃SO₃, which leads to a reduction in the intensity of PEO peaks at 19.19° and 23.63°. This signifies the disruption of the organized patterns of the PEO chains, namely the layered structure of the crystalline portion of the polymer. The presence of an undefined improvement in the PEO-LiCF₃SO₃ polymer blend system would impact the conductive properties of the samples [28]. The formation of the amorphous phase leads to a decrease in the energy barrier for the movement of polymer chain segments. Consequently, the conductivity rises proportionally to the expansion of the amorphous region inside the sample. It is expected that the specimen with the largest amorphous region would have the best electrical conductivity at room temperature.

The strength of the crystalline peak exhibits a significant drop when the concentration of LiCF₃SO₃ is 8 wt.%. This observation indicates that the structure of PEO may be transformed into an amorphous state in certain regions by raising the concentration of LiCF₃SO₃ till 8 wt.% of concentration, after that no peaks appears. Therefore, it is anticipated that the overall ionic conductivity in the surrounding environment would be higher in comparison to PEO. The introduction of LiCF₃SO₃

disrupted the ordering in the PEO as a result of coordination interactions between Li⁺ ions and the ether atom [29]. Moreover, Johan *et al.* [30] asserted that the addition of salt leads to a significant drop in the intensities of the PEO peaks. This decrease is attributed to the enhanced amorphous characteristics of the polymer electrolytes.

PEO-Ni/Al LDH-LiCF₃SO₃: The XRD patterns of the PEO-FNi/Al LDH and CNi/Al LDH at 5 wt.% LiCF₃SO₃ is shown in Fig. 5. The two strong diffraction peaks at 19.19° and 23.63° indicate the crystallinity phase of PEO in the electrolyte system [31]. There is a significant decrease in the intensity of peak as the LiCF₃SO₃ salt concentration increases, which results in the increment of overall non-crystalline region within the electrolyte system, mostly caused by the disruption of the dopant on the layered structure of PEO. Ahmed *et al.* [32] proposed that this leads to a decrease in the entropy of the systems as observed in a comparable PEO electrolyte system. Owing to the homogeneous dispersion of LiCF₃SO₃ in the PEO-Ni/Al LDH and the distribution of ordered arrangement of the polymer side chain, reducing the crystallinity of the electrolyte solution is a favorable strategy to improve ion mobility [33]. Therefore, an increase in ionic conductivity for the system is expected.

Fourier transform infrared (FTIR) of the systems

PEO-Ni/Al LDH: The vibrational modes and wavenumbers exhibited by PEO are CH₂ rocking mode observed at 839 and 953 cm⁻¹, the strongest mode in PEO is antisymmetric bridge C-O-C stretching at 1100 cm⁻¹, asymmetric CH₂ twisting at 1241 and 1278 cm⁻¹ and asymmetric CH₂ at 1464 cm⁻¹ (Fig. 6). Other transmittance bands are observed for symmetric and asymmetric C-H stretching vibrations at 3000–2800 cm⁻¹ and 2800–2700 cm⁻¹, respectively [26,34,35]. The band appears at 3504 cm⁻¹ is attributed to the presence of moisture which is due to the hydrophilic nature of PEO [36]. Table-1 summarized key infrared wavenumbers and vibrational modes of PEO.

Fig. 7 depicts the interaction between PEO and Ni/Al LDH and no noticeable coordination was observed between the PEO and Ni/Al LDH. This is due to the absence of any detected alter-

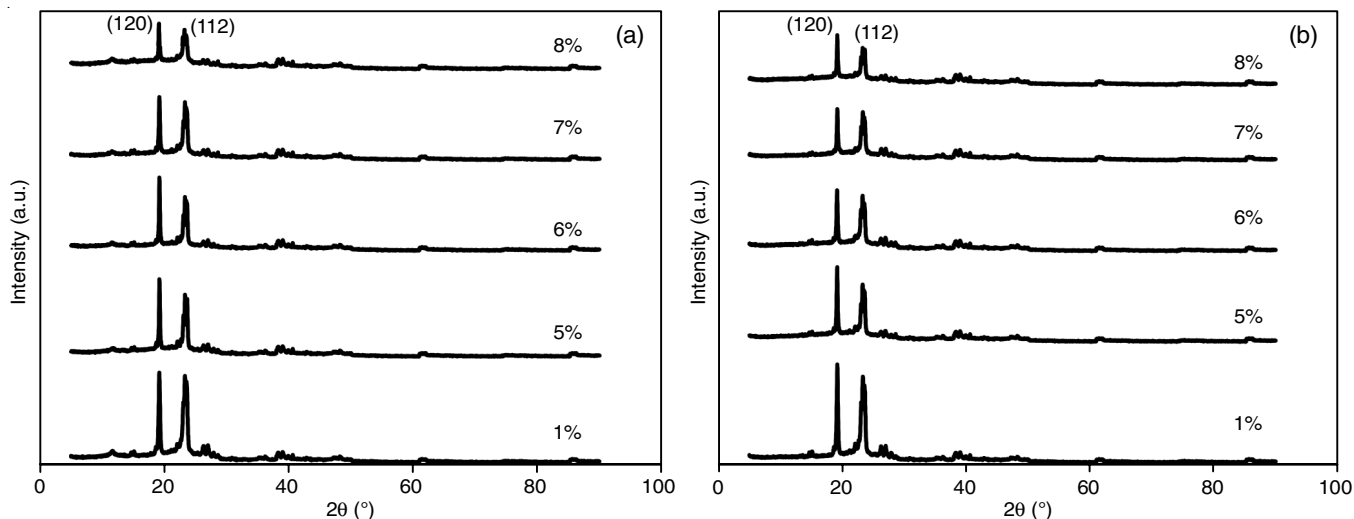


Fig. 5. X-ray diffraction patterns of (a) PEO-FNi/Al LDH-LiCF₃SO₃ and (b) PEO-CNi/Al LDH-LiCF₃SO₃

TABLE-1
KEY INFRARED WAVE NUMBERS AND VIBRATIONAL MODES OF PEO

Characteristics frequencies	Characteristics band	Wavenumbers (cm ⁻¹) (this study)	Wavenumbers (cm ⁻¹) (Literature)	Ref.
PEO	Asymmetric C-H stretching	3504	2700–3800	[37]
	Symmetric CH ₂	2878	2800–3000	[30]
	Asymmetric CH ₂	1464, 1340	1455	[38]
	Asymmetric CH ₂ twisting	1278	1241 and 1280	[31]
	Antisymmetric bridge C-O-C stretching	1100	1100	[29]
	CH ₂ rocking mode	839 and 953	842 and 963	[39]

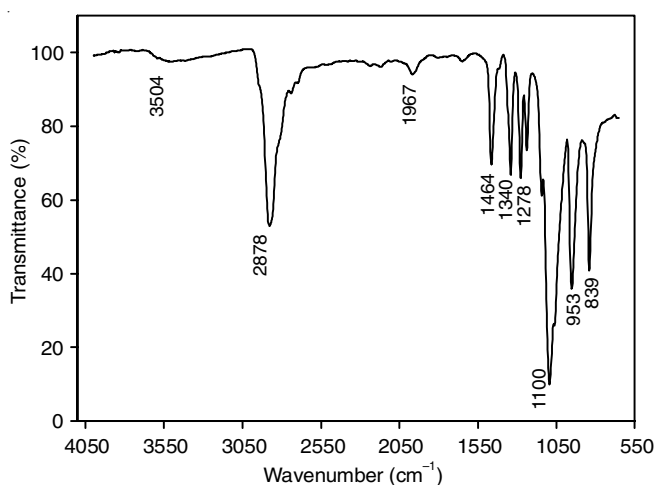
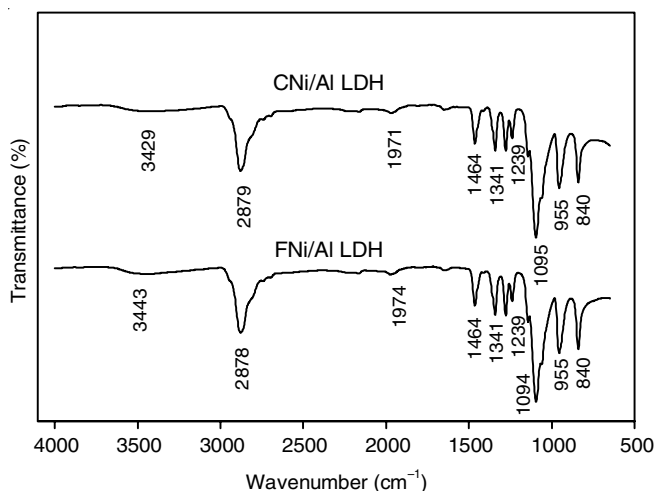


Fig. 6. Infrared spectra of PEO


 Fig. 7. Infrared spectral bands (cm⁻¹) of PEO for FNi/Al LDH and CNi/Al LDH, respectively

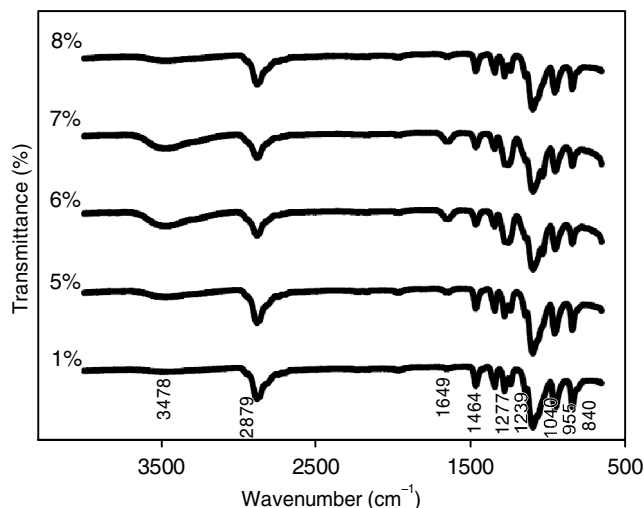
ations in the transmission peak within the spectrum. It is evident that the Ni/Al LDH is incompatible with PEO and produces films with different properties at room temperature.

A broad absorption bands at 3443 cm⁻¹ and 3429 cm⁻¹ in the FTIR spectrum of PEO- Ni/Al LDH can be assigned to the stretching vibration of the hydroxyl groups of LDH layers and intercalated or adsorbed water molecules. The bands at 3443 cm⁻¹ and 3429 cm⁻¹ show a significant shift in the spectrum, which mainly due to the presence of moisture in the system indicating the hydrophilic nature of PEO [20]. Table-2 summarizes key infrared wave numbers and vibrational modes of PEO-Ni/Al LDH.

TABLE-2
KEY INFRARED WAVE NUMBERS AND VIBRATIONAL MODES OF PEO-Ni/Al LDH

Materials	Characteristics band	Wavenumber (cm ⁻¹) (This study)
PEO-FNi/Al LDH	O-H stretching	3443
	Symmetric CH ₂	2878
	Asymmetric CH ₂	1464, 1341
	Asymmetric CH ₂ twisting and C-O-C stretching	1239, 1094
	CH ₂ rocking mode	955, 840
	O-H stretching	3429
	Symmetric CH ₂	2879
	Asymmetric CH ₂	1464, 1341
	Asymmetric CH ₂ twisting and C-O-C stretching	1239, 1095
	CH ₂ rocking mode	955, 840

PEO-LiCF₃SO₃: The interaction and coordination of PEO-LiCF₃SO₃ was also interpreted with FTIR technique as shown in Fig. 8. The fingerprint peaks for LiCF₃SO₃ occur at 1256 cm⁻¹ ν_s (CF₃), 1190 cm⁻¹ ν_{as} (CF₃) and 1040 cm⁻¹ ν_s (SO₃) are same as reported earlier [40]. The triflate ion exhibits high sensitivity to the atoms in its vicinity, which is attributed to variations in the electronegativity. These variations, in turn, altered the vibration mode of ion. The PEO displays the vibrational peaks at 758, 1029 and 1232 cm⁻¹, which correspond to the interactions between LiCF₃SO₃. These peaks experience a significant changes in both intensity and location as the salt concentration increases [41]. The peaks at 3484 cm⁻¹ and 1642 cm⁻¹ in pure LiCF₃SO₃ is disappeared in the complex, sugge-


 Fig. 8. Infrared spectra of PEO at different LiCF₃SO₃ concentration

sting the occurrence of coordination between the salt and polymer (Table-3) [36].

The FTIR spectrum of PEO-LiCF₃SO₃ has three distinct peaks at 1277, 1144 and 1040 cm⁻¹. The presence of ether-oxygen cation interaction is shown by the altered stretching vibration of the C-O-C bond and the shift in peak positions compared to pure PEO [28]. The peak at 1239 cm⁻¹ (CF₃) is displaced to 1277 cm⁻¹ at its highest point, which is due to the interaction between PEO and LiCF₃SO₃ caused by the alteration of triflate ions in the complex. The C-H stretching frequency of PEO, first observed at 2878 cm⁻¹ shifted to 2879 cm⁻¹ in the complex. Pure PEO asymmetric bending vibration at 1455 cm⁻¹ was red-shifted to 1649 cm⁻¹ in the polymer complex [36] and the peak intensity became broader. The peak at 3442 cm⁻¹ in pure PEO is displaced to 3478 cm⁻¹ due to the development of a complex between the lithium salt and the polymer host. The coordination of LiCF₃SO₃ cations with the etheral oxygen of PEO is thought to be responsible for the observed spectrum alterations, which are attributed to the impact of LiCF₃SO₃ or the stretching and distortion of the C-O-C bond. Water may be detected by a prominent peak in the range of 3600-3200 cm⁻¹, which corresponds to the -OH stretching vibrational mode [41].

PEO-Ni/Al LDH-LiCF₃SO₃: Fig. 9 demonstrates the interaction between PEO-5 wt.% FNi/Al LDH-LiCF₃SO₃ and

PEO-5 wt.% CNi/Al LDH-LiCF₃SO₃ at varying weight percentages. PEO displays the vibrational modes and wavenumbers corresponding to the CH₂ rocking modes at 954 and 840 cm⁻¹ [41]. The interaction between FNi/Al LDH is associated with the lattice vibration modes of M-O, O-M-O and M-O-M as shown by the peak at 854 cm⁻¹ [42]. The peak at 1040 cm⁻¹ in LiCF₃SO₃ has been displaced to 1031 cm⁻¹, which corresponds to the stretching vibration of the C-O-C bond. Additionally, the positions of the peaks have altered compared to pure PEO indicating an interaction between the ether oxygen and the cation. It may also be attributed to the symmetric stretching of free triflate ion, which is sensitive to the dissociation of lithium salt because of weak ion pairing between the cation (Li⁺) and anion (CF₃SO₃⁻) in the metal salt [43].

The peaks corresponding to the stretching mode of C-O-C at 1100 cm⁻¹ also shifted to 1095 cm⁻¹ when Ni/Al LDH is added [30]. The intensity of the peaks within the range of 1276 to 1249 cm⁻¹ is weakened indicating the occurrence of complexation between PEO, LiCF₃SO₃ and FNi/Al LDH. The interaction between PEO, LiCF₃SO₃ and CNi/Al LDH occurred within the spectral range of 1275 to 1251 cm⁻¹ resulting in a decrease in intensity. The interactions between PEO, LiCF₃SO₃ and Ni/Al LDH are shown at 1465 and 1343 cm⁻¹. This suggests that the presence of the system progressively decreases the concen-

TABLE-3
KEY INFRARED WAVENUMBERS AND VIBRATIONAL MODES OF PEO-LiCF₃SO₃

Characteristics frequencies	Characteristics band	Wavenumbers (cm ⁻¹) (This study)	Wavenumbers (cm ⁻¹) (reference)	Ref.
LiCF ₃ SO ₃	(ν _s (CF ₃))		1256	[40]
	(ν _{as} (CF ₃))		1190	[40]
	(ν _s (SO ₃))		1040	[40]
	δ _s (CF ₃)		775	[40]
	OH ⁻ stretching vibrational	3478	3600-3200	[30]
PEO-LiCF ₃ SO ₃	Symmetric CH ₂	2879	3000-2800	[30]
	Asymmetric CH ₂	1649, 1464	1455	[38]
	(ν _s (CF ₃)) Asymmetric CH ₂ twisting	1277, 1239	1280 and 1241	[31]
	Antisymmetric bridge C-O-C stretching	1040	1100	[29]
	CH ₂ rocking mode	955 and 840	963 and 842	[39]

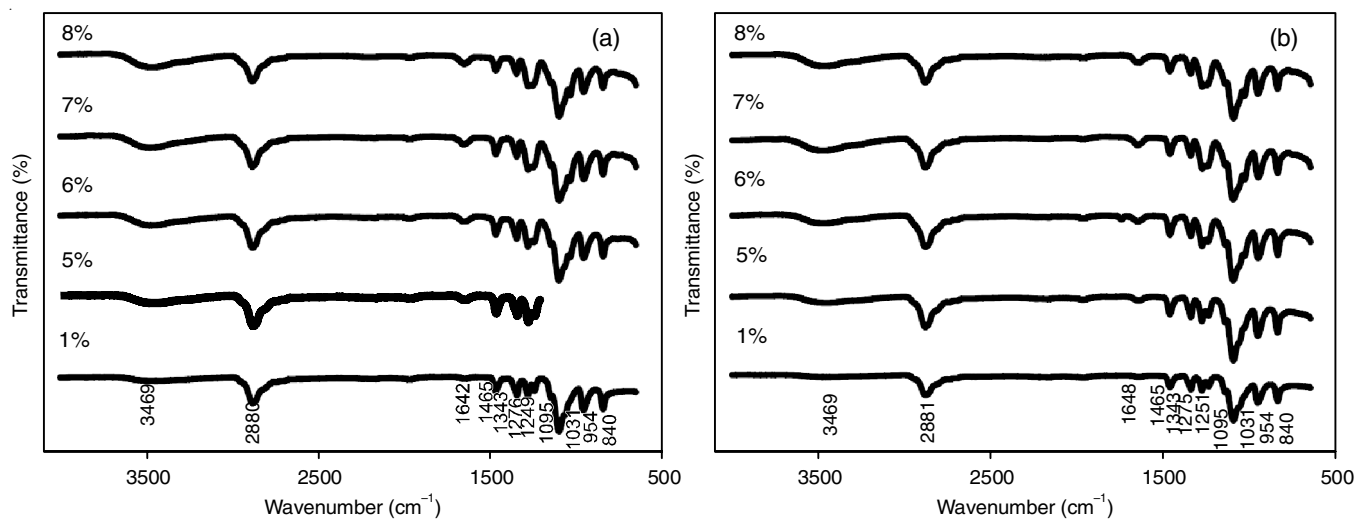


Fig. 9. Infrared spectra of PEO-5 wt.% (a) FNi/Al LDH and (b) CNi/Al LDH at different wt.% LiCF₃SO₃

tration of free Li^+ ions *via* interactions [30]. The interaction of LiCF_3SO_3 with Ni/Al LDH leads to a progressive decrease in the intensity at 1464 and 1343 cm^{-1} , which are associated with the crystalline phase of PEO [43].

The interaction of PEO-FNi/Al LDH with increasing concentrations of salts is appeared at 1642 cm^{-1} . The PEO-CNi/Al LDH has broad peak at 1648 cm^{-1} , which becomes more broader as the salt concentration increases. The PEO-Ni/Al LDH- LiCF_3SO_3 also exhibits at the specific wavenumbers of 2881 and 2880 cm^{-1} , respectively, which suggests that the presence of system progressively decreases the concentration of free Li^+ ions *via* interactions [30]. The detection of moisture may be determined by the alterations in the 3600-3200 cm^{-1} range, which is due of the OH-stretching vibrational mode. The spectrum of LiCF_3SO_3 has a distinct peak at 3469 cm^{-1} , which corresponds to the OH-stretching mode of hydrogen bonding. The observed phenomena in the LiCF_3SO_3 electrolyte system may be attributed to the hygroscopic nature of this inorganic salt [30]. The important vibrational modes and infrared wavenumbers are shown in Table-4.

Field emission scanning electron microscope (FESEM)

PEO-Ni/Al LDH: The shape of both the polymer matrix and filler significantly affects the mechanical, thermal, ionic conductivity and interface characteristics of the PEO-based composite electrolytes [44]. Fig. 10a displays the surface picture of the PEO film in its unadulterated state. The images depict a coarse structure at a magnification of 200X exhibiting many

micropores. This is a typical observation for PEO-based electrolytes that are produced using the solution casting technique. The formation of these tiny holes is a result of rapid evaporation of ACN solvent during the process of sample preparation. Fig. 10b-c depicts the images of PEO-FNi/Al LDH in and PEO-CNi/Al LDH. The PEO-FNi/Al LDH exhibited a rough surface with a flake-like structure and numerous pores, whereas the rough surface of PEO-CNi/Al LDH is characterized by sand roses, petal plates and irregular forms.

The overall amorphous area of the PEO-FNi/Al LDH and PEO-CNi/Al LDH is lower than the crystallinity phase of the system. Moreover, it might be suggested that there is a lack in the interaction between the PEO and LDH, hence, the PEO-Ni/Al LDH systems exhibit incompatibility. The XRD analysis confirmed that no changes observed in the system before and after the addition of LDH.

PEO- LiCF_3SO_3 : It is evident that distribution of LiCF_3SO_3 affects the complexation of PEO, which in turn forces the continuous crystals to break down and the lamellar dimension to be lowered (Fig. 11). An increase in the roughness level with higher LiCF_3SO_3 concentration suggests the separation of dopant inside the matrix. Dhatarwal & Sengwa [41] asserted that the production of a blended polymer is due to the creation of a crosslinked chain structure as regulated by the ion-dipole interactions with lithium cations. Moreover, it displays bigger spherulites and fibril-like textures, which are indicative of the crystallites observed in PEO. These textures also suggest the presence of extensive interface areas, which contribute to the

TABLE-4
KEY INFRARED BANDS (cm^{-1}) AND VIBRATIONAL MODES OF PEO-Ni/Al LDH- LiCF_3SO_3

Characteristics frequencies	Characteristics band	Wavenumbers (cm^{-1}) (This study)
PEO-FNi/Al LDH- LiCF_3SO_3	OH-stretching mode	3469
	Symmetric CH_2	2880
	Asymmetric CH_2	1642, 1465
	Asymmetric CH_2 twisting	1276, 1249
	C-O-C stretching mode	1095, 1031
	CH_2 rocking mode & lattice vibration mode	954-840
PEO-CNi/Al LDH- LiCF_3SO_3	OH-stretching mode	3469
	Symmetric CH_2	2881
	Asymmetric CH_2	1648, 1465
	Asymmetric CH_2 twisting	1275, 1251
	C-O-C stretching mode	1095, 1031
	CH_2 rocking mode & lattice vibration mode	954, 840

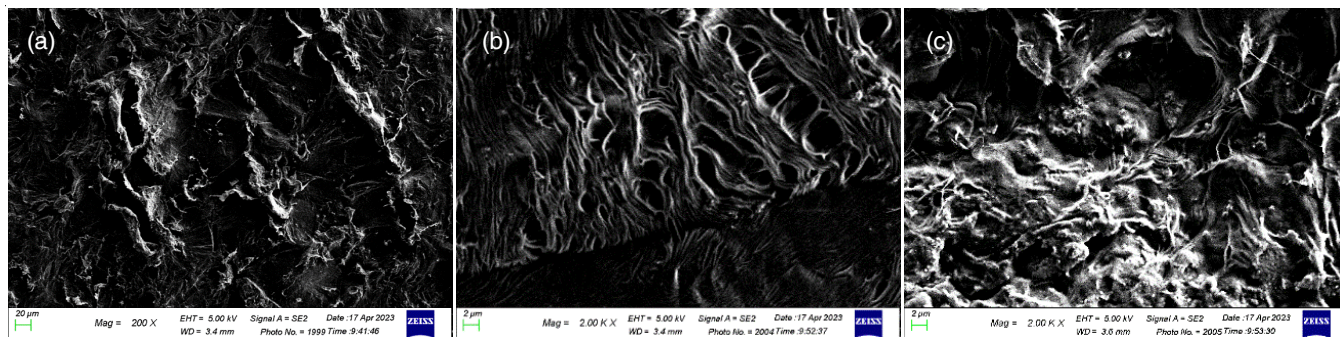
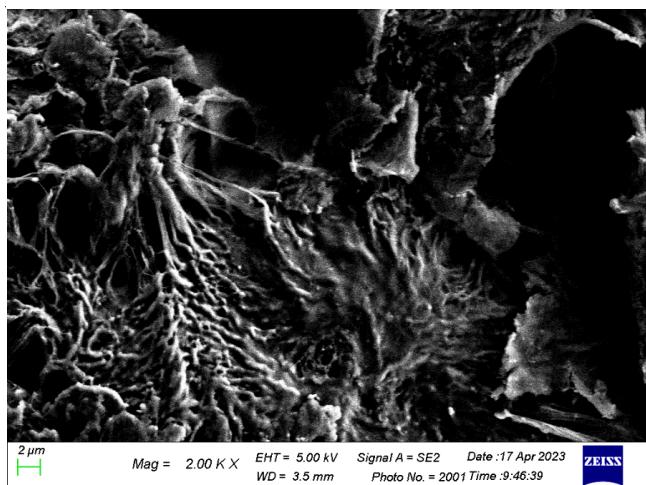


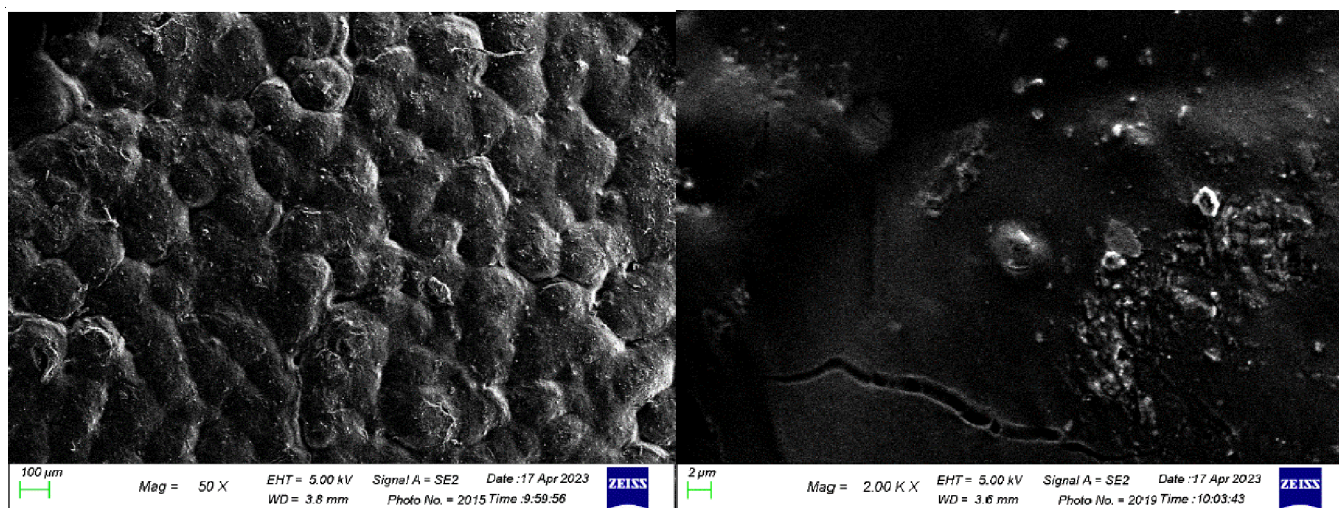
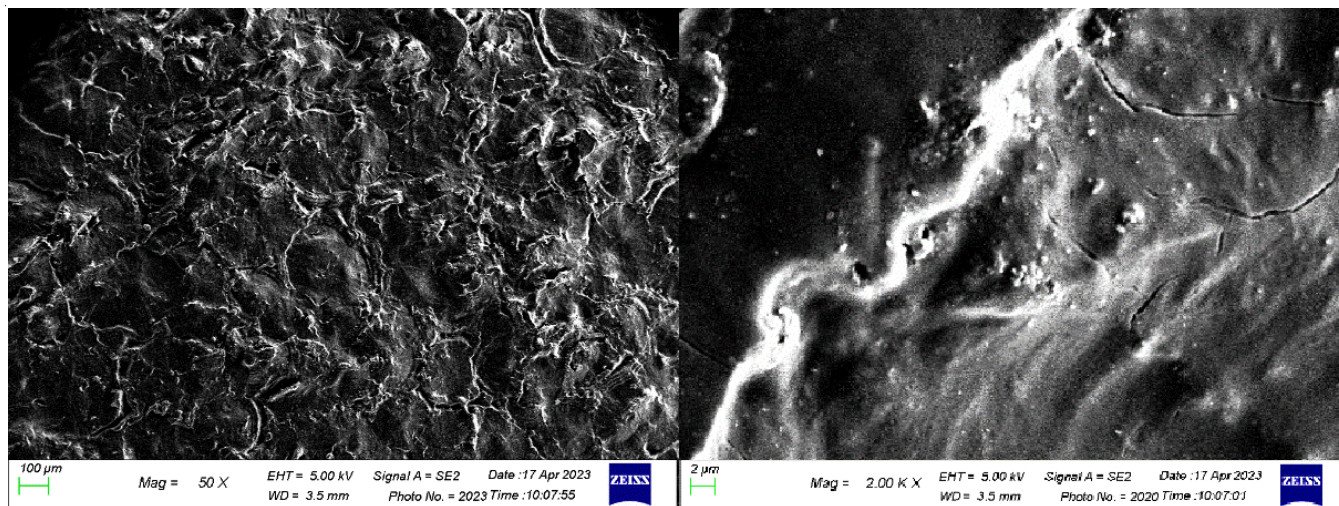
Fig. 10. FE-SEM images of (a) PEO, (b) PEO-FNi/Al LDH and (c) PEO-CNi/Al LDH

Fig. 11. FE-SEM images of PEO-8 wt.% LiCF_3SO_3

amorphous portion of the PEO system. The XRD analysis supports the inclusion of LiCF_3SO_3 in the PEO system, which has expanded the overall range of amorphous characteristics in the electrolyte at room temperature.

PEO-Ni/Al LDH- LiCF_3SO_3 : A highly porous surface with clearly defined boundaries between the spherulites in PEO-5 wt.% FNi/Al LDH and 8 wt.% LiCF_3SO_3 is visible in Fig. 12. The average dimensions and morphology of spherulites vary depending on the concentration of salt [33]. It is significant that the surface becomes smoother and the spherulite texture completely disappears as observed at 2K magnification. The alterations were caused by the positive impact of FNi/Al LDH and LiCF_3SO_3 on reducing the crystallinity of PEO and increasing the amorphous percentage in the SPEs. The presence of a smooth structure in the electrolyte samples is linked to the improvement of the amorphous phase and may enhance the movement of ions, leading to an increase in the ionic conductivity of the system [43].

The incorporation of 8 wt.% of LiCF_3SO_3 demonstrates the uniformity of PEO-5 wt.% CNi/Al LDH, since no segregation of phases is observed (Fig. 13). The enhancement of surface morphology may be seen as the introduction of salt upon it. The wrinkles in the PEO decreases and transformed the rough surface into a smooth one due to the addition of salt, thus helps in the elevation of ionic conductivity [20].

Fig. 12. FE-SEM images of PEO-5 wt.% FNi/Al LDH-8 wt.% LiCF_3SO_3 Fig. 13. FE-SEM images of PEO-5 wt.% CNi/Al LDH-8 wt.% LiCF_3SO_3

Electrochemical studies of PEO system

PEO–Ni/Al LDH: A free-standing film composed of PEO and Ni/Al LDH was prepared at ambient temperature. Then, PEO with different wt.% of FNi/Al LDH and CNi/Al LDH were prepared by dissolving in ACN. Fig. 14 shows the ionic conductivity (σ) of FNi/Al LDH and CNi/Al LDH at ambient temperature. In overall, it shows that the ionic conductivity of CNi/Al LDH is higher than FNi/Al LDH and the optimum ionic conductivity for both system was observed at 5 wt.%. The ionic conductivity of PEO–CNi/Al LDH and PEO–FNi/Al LDH system was 8.93×10^{-9} S cm $^{-1}$ and 6.89×10^{-9} S cm $^{-1}$, respectively. However, there is no significant difference in the ionic conductivity for both the system, since both have the same order of magnitude and also no substantial improvement in the ionic conductivity before addition of LDH was observed. Thus, it may be inferred that LDH does not contribute to the enhancement of the ionic conductivity in the system, which is mainly due to the properties of the Ni/Al LDH itself. Taoufik *et al.* [45] reported that upon calcination, the CNi/Al LDH experienced the structural collapse resulting in the formation of NiO as verified by the XRD analysis. The textural properties for the specific surface areas and pore size significantly affect the ionic conductivity. The error bar data from this experiment falls within the range of the conductivity measurements. A 95% confidence interval was generated by calculating the error bar using the standard deviation method applied to the average conductivity data. Due to the small margin of error ($> 2\%$), all the conductivity measurements in this study follow the same protocol.

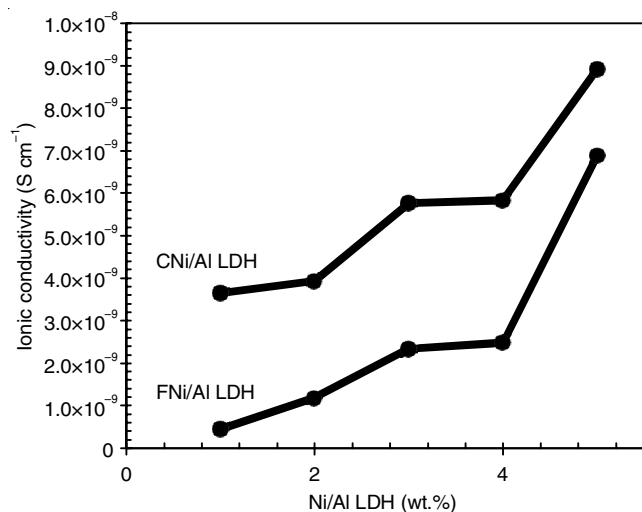


Fig. 14. Ionic conductivity of PEO–Ni/Al LDH

PEO–LiCF $_3$ SO $_3$: The solvent casting method was utilized to prepare 1.0 g PEO having different weight percent LiCF $_3$ SO $_3$ dissolved in ACN. Fig. 15 shows the variation in conductivity with different wt.% of LiCF $_3$ SO $_3$ and the highest conductivity value of 4.93×10^{-6} S cm $^{-1}$ in this system was obtained at 8% of LiCF $_3$ SO $_3$. However, at higher composition of 9% LiCF $_3$ SO $_3$, the PEO–LiCF $_3$ SO $_3$ system films and remains in the gel state. Klolygon & Pumchusak [31] reported that the presence of water molecules in the PEO–20% LiCF $_3$ SO $_3$ membrane resulted in

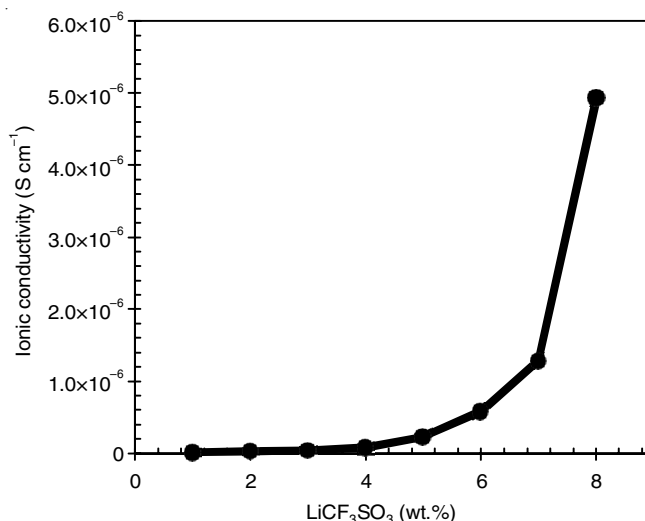


Fig. 15. Ionic conductivity of PEO with different wt.% of LiCF $_3$ SO $_3$

the reduction of ionic conductivity. Since LiCF $_3$ SO $_3$ has a high affinity for water molecules, making it excellent water absorber. At a concentration of 20% LiCF $_3$ SO $_3$ in PEO, the moisture was being absorbed, resulting in an increase in the mobility of the PEO–LiCF $_3$ SO $_3$ system. Consequently, the water molecules establish hydrogen bonds with PEO impeding the creation of connections between PEO and LiCF $_3$ SO $_3$ systems [31].

PEO–Ni/Al LDH–LiCF $_3$ SO $_3$: From Fig. 16, it clearly shows the PEO–5 wt.% of CNi/Al LDH–8 wt.% of LiCF $_3$ SO $_3$ has higher conductivity which is 8.35×10^{-6} cm $^{-1}$ compared to the PEO–5 wt.% of FNi/Al LDH–8 wt.% of LiCF $_3$ SO $_3$ which is 5.74×10^{-6} cm $^{-1}$. At 1 wt.% of LiCF $_3$ SO $_3$, the ionic conductivity of this system shown slight better conductivity and with FNi/Al LDH and CNi/Al LDH, the ionic conductivity were 1.07×10^{-8} and 1.42×10^{-8} , respectively. With 5 wt.% of LiCF $_3$ SO $_3$, the ionic conductivity shows the improvement which indicated that higher wt.% of LiCF $_3$ SO $_3$ into the PEO–Ni/Al LDH, the higher ionic conductivity of the system. However, at 9 wt.% of LiCF $_3$ SO $_3$, the ionic conductivity decreases which is attributed due to higher viscosity of the membrane. Thus at the optimum conditions, FNi/Al LDH and CNi/Al LDH

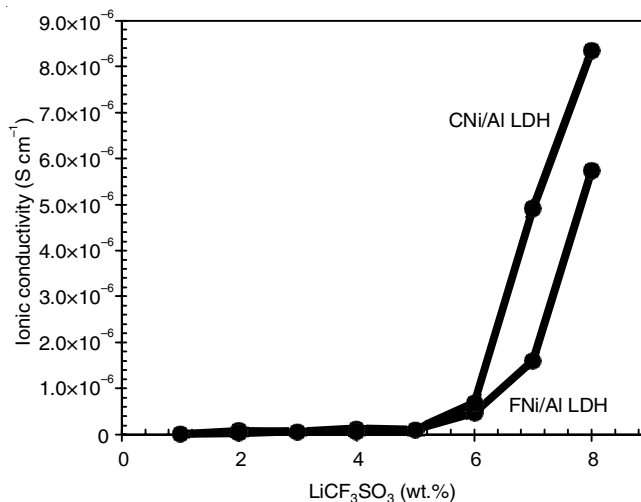


Fig. 16. Ionic conductivity of PEO–Ni/Al LDH–LiCF $_3$ SO $_3$

dissociate the lithium salt resulting in an enhancement of the ionic conductivity [36].

The conductivity measurement in Fig. 16 was interrupted at 8 wt.%, which could be because ion pairing formed in the electrolyte system. Ion aggregation, in which Li^+ and CF_3SO_3^- ions paired together to restrict the migration of Li^+ ions and lower the ion conducting channel and a decrease in the number of effective charge carriers cause the decrease in the ionic conductivity below 8% concentration [28,36]. Thus, the PEO–5 wt.% FNi/Al LDH–8 wt.% LiCF_3SO_3 and PEO–5 wt.% CNi/Al LDH–8 wt.% LiCF_3SO_3 to be optimal in tuning the ionic conductivity.

Conclusion

In this work, ternary solid polymer electrolytes based on poly(ethylene)oxide doped with lithium trifluoromethane sulfonate (LiCF_3SO_3) containing Ni/Al layered double hydroxide as filler with improved ionic conductivities were prepared by solvent casting method. The addition of 5 wt.% CNi/Al LDH and 8 wt.% LiCF_3SO_3 to PEO results in a significantly higher conductivity of $8.35 \times 10^{-6} \text{ S cm}^{-1}$ compared to the conductivity of pure PEO which is only $1.76 \times 10^{-9} \text{ S cm}^{-1}$. The XRD and FTIR analyses indicate reduced crystallinity and complexation, while the FESEM examination verifies that the films exhibit enhanced smoothness and increased porosity. The use of Ni/Al LDH as a filler effectively improves both the interactions and ionic conductivity within the electrolyte system.

CONFLICT OF INTEREST

The authors declare that there is no conflict of interests regarding the publication of this article.

REFERENCES

- J. Yue, L. Lin, L. Jiang, Q. Zhang, Y. Tong, L. Suo, Y. Hu, H. Li, X. Huang and L. Chen, *Adv. Energy Mater.*, **10**, 2000665 (2020); <https://doi.org/10.1002/aenm.202000665>
- L. Qiao, X. Judez, T. Rojo, M. Armand and H. Zhang, *J. Electrochem. Soc.*, **167**, 070534 (2020); <https://doi.org/10.1149/1945-7111/ab7aa0>
- M.B. Armand, *Ann. Rev. Mater. Sci.*, **16**, 245 (1986); <https://doi.org/10.1146/annurev.ms.16.080186.001333>
- J. Yang, F. Gu and J. Guo, *Resour. Conserv. Recycling*, **156**, 104713 (2020); <https://doi.org/10.1016/j.resconrec.2020.104713>
- E. Fan, L. Li, Z. Wang, J. Lin, Y. Huang, Y. Yao, R. Chen and F. Wu, *Chem. Rev.*, **120**, 7020 (2020); <https://doi.org/10.1021/acs.chemrev.9b00535>
- I. Aldalur, X. Wang, A. Santiago, N. Goujon, M. Echeverría, M. Martínez-Ibañez, M. Piszcz, P.C. Howlett, M. Forsyth, M. Armand and H. Zhang, *J. Power Sources*, **448**, 227424 (2020); <https://doi.org/10.1016/j.jpowsour.2019.227424>
- P.V. Wright, *Electrochim. Acta*, **43**, 1137 (1998); [https://doi.org/10.1016/S0013-4686\(97\)10011-1](https://doi.org/10.1016/S0013-4686(97)10011-1)
- B. Jinisha, A.F. Femy, M.S. Ashima and S. Jayalekshmi, *Mater. Today Proc.*, **5**, 21189 (2018); <https://doi.org/10.1016/j.matpr.2018.06.518>
- V.P. Hoang Huy, S. So and J. Hur, *Nanomaterials*, **11**, 1 (2021); <https://doi.org/10.3390/nano11030614>
- J.P. Sharma and V. Singh, *High Perform. Polym.*, **32**, 142 (2020); <https://doi.org/10.1177/0954008319894043>
- Y. Mallaiyah, V.R. Jeedi, R. Swarnalatha, A. Raju, S.N. Reddy and A.S. Chary, *J. Phys. Chem. Solids*, **155**, 110096 (2021); <https://doi.org/10.1016/j.jpcs.2021.110096>
- N. Boaretto, L. Meabe, M. Martínez-Ibañez, M. Armand and H. Zhang, *J. Electrochem. Soc.*, **167**, 070524 (2020); <https://doi.org/10.1149/1945-7111/ab7221>
- X. Cheng, J. Pan, Y. Zhao, M. Liao, and H. Peng, *Adv. Energy Mater.*, **8**, 1702184 (2018); <https://doi.org/10.1002/aenm.201702184>
- S.N. Banitaba, D. Semnani, B. Rezaei and A.A. Ensafi, *Polym. Adv. Technol.*, **30**, 1234 (2019); <https://doi.org/10.1002/pat.4556>
- W.Q. Ding, F. Lv, N. Xu, M.T. Wu, J. Liu and X.P. Gao, *ACS Appl. Energy Mater.*, **4**, 4581 (2021); <https://doi.org/10.1021/acs.aem.1c00216>
- J. Mindemark, M.J. Lacey, T. Bowden and D. Brandell, *Prog. Polym. Sci.*, **81**, 114 (2018); <https://doi.org/10.1016/j.progpolymsci.2017.12.004>
- S.N.A.M. Johari, N.A. Tajuddin, H. Hanibah and S.K. Deraman, *Int. J. Electrochem. Sci.*, **16**, 211049 (2021); <https://doi.org/10.20964/2021.10.53>
- I.M. Noor, *High Perform. Polym.*, **32**, 168 (2020); <https://doi.org/10.1177/0954008319890016>
- L. Valeikiene, R. Paitian, I. Grigoraviciute-Puroniene, K. Ishikawa and A. Kareiva, *Mater. Chem. Phys.*, **237**, 121863 (2019); <https://doi.org/10.1016/j.matchemphys.2019.121863>
- S.K. Patla, R. Ray, K. Asokan and S. Karmakar, *J. Appl. Phys.*, **123**, 125102 (2018); <https://doi.org/10.1063/1.5022050>
- R. Fang, B. Xu, N.S. Grundish, Y. Xia, Y. Li, C. Lu, Y. Liu, N. Wu and J.B. Goodenough, *Angew. Chem. Int. Ed.*, **60**, 17701 (2021); <https://doi.org/10.1002/anie.202106039>
- S. Wrede, B. Cai, A. Kumar, S. Ott and H. Tian, *J. Am. Chem. Soc.*, **145**, 11472 (2023); <https://doi.org/10.1021/jacs.3c01333>
- R. Cuana, T.I. Nasution, H. Agusnar, A. Susilowati, N.S. Lubis and I.S. Pradana, *J. Physics: Conf. Ser.*, **2421**, 012038 (2023); <https://doi.org/10.1088/1742-6596/2421/1/012038>
- M. Wang, M.Y. Tan, Y. Zhu, Y. Huang and Y. Xu, *NPJ Mater. Degrad.*, **7**, 16 (2023); <https://doi.org/10.1038/s41529-023-00332-x>
- D.R. Joshi and N. Adhikari, *J. Pharm. Res. Int.*, **28**, 1 (2019); <https://doi.org/10.9734/jpr/2019/v28i330203>
- M.S. Mustafa, H.O. Ghareeb, S.B. Aziz, M.A. Brza, S. Al-Zangana, J.M. Hadi and M.F.Z. Kadir, *Membranes*, **10**, 116 (2020); <https://doi.org/10.3390/membranes10060116>
- W.S. Young, J.N.L. Albert, A.B. Schantz and T.H. Epps III, *Macromolecules*, **44**, 8116 (2011); <https://doi.org/10.1021/ma2013157>
- P. Pongsuk and J. Pumchusak, *Mater. Today Proc.*, **17**, 1956 (2019); <https://doi.org/10.1016/j.matpr.2019.06.241>
- S. Klongkan and J. Pumchusak, *Electrochim. Acta*, **161**, 171 (2015); <https://doi.org/10.1016/j.electacta.2015.02.074>
- M.R. Johan, O.H. Shy, S. Ibrahim, S.M. Mohd Yassin and T.Y. Hui, *Solid State Ion.*, **196**, 41 (2011); <https://doi.org/10.1016/j.ssi.2011.06.001>
- S. Klongkan and J. Pumchusak, *Int. J. Chem. Eng. Appl.*, **6**, 165 (2015); <https://doi.org/10.7763/IJCEA.2015.V6.474>
- H.T. Ahmed and O.G. Abdullah, *Polymers*, **11**, 853 (2019); <https://doi.org/10.3390/polym11050853>
- J. Gurusiddappa, W. Madhuri, R. Padma Suvarna and K. Priya Dasan, *Mater. Today Proc.*, **3**, 1451 (2016); <https://doi.org/10.1016/j.matpr.2016.04.028>
- A.M. Abdelghany, M.O. Farea and A.H. Oraby, *J. Mater. Sci. Mater. Electron.*, **32**, 6538 (2021); <https://doi.org/10.1007/s10854-021-05371-1>
- L. Lin, Y. Zhu, C. Li, L. Liu, D. Surendhiran and H. Cui, *Carbohydr. Polym.*, **198**, 225 (2018); <https://doi.org/10.1016/j.carbpol.2018.06.092>
- A.J. Nagajothi, R. Kannan and S. Rajashabala, *Mater. Sci. Pol.*, **36**, 185 (2018); <https://doi.org/10.1515/msp-2018-0025>
- P. Dhatarwal and R.J. Sengwa, *Polym. Bull.*, **75**, 5645 (2018); <https://doi.org/10.1007/s00289-018-2354-6>

38. S. Malhotra and P.K. Varshney, *Int. J. Appl. Eng. Res.*, **10**, 108 (2015).
39. S. Choudhary and R.J. Sengwa, *Electrochim. Acta*, **247**, 924 (2017); <https://doi.org/10.1016/j.electacta.2017.07.051>
40. S.M. Mohd Yasin and M.R. Johan, *Malays. Nano-Int. J.*, **1**, 1 (2021); <https://doi.org/10.22452/mnij.vol1no1.1>
41. P. Dhatarwal and R.J. Sengwa, *Ionics*, **26**, 2259 (2020); <https://doi.org/10.1007/s11581-019-03337-2>
42. Z. Lv, S. Yang, H. Zhu, L. Chen, N.S. Alharbi, M. Wakeel, A. Wahid and C. Chen, *Appl. Surf. Sci.*, **448**, 599 (2018); <https://doi.org/10.1016/j.apsusc.2018.04.162>
43. S.A. Suthanthiraraj and M.K. Vadivel, *Appl. Nanosci.*, **2**, 239 (2012); <https://doi.org/10.1007/s13204-012-0099-3>
44. C. Bhatt, R. Swaroop, A. Arya and A.L. Sharma, *J. Mater. Sci. Eng. B*, **5**, 418 (2015); <https://doi.org/10.17265/2161-6221/2015.11-12.003>
45. N. Taoufik, W. Boumya, A. Elhalil, M. Achak, M. Sadiq, M. Abdennouri and N. Barka, *Int. J. Environ. Anal. Chem.*, **103**, 712 (2021); <https://doi.org/10.1080/03067319.2020.1863387>